Preferred citation: M. Mettänen, U. Hirn, M. Lauri and R. Ritala. Probabilistic analysis of small-scale print defects with aligned 2D measurements. In **Advances in Pulp and Paper Research, Oxford 2009**, *Trans. of the XIVth Fund. Res. Symp. Oxford, 2009*, (S.J. I'Anson, ed.), pp 1293–1323, FRC, Manchester, 2018. DOI: 10.15376/frc.2009.2.1293.

PROBABILISTIC ANALYSIS OF SMALL-SCALE PRINT DEFECTS WITH ALIGNED 2D MEASUREMENTS

Marja Mettänen[1], Ulrich Hirn[2], Mikko Lauri[3] and Risto Ritala[4]

[1,3,4]Department of Automation Science and Engineering, Tampere University of Technology, P.O. Box 692, 33101 Tampere, Finland, [2]Institute of Paper, Pulp and Fibre Technology, Graz University of Technology, Kopernikusgasse 24, 8010 Graz, Austria

ABSTRACT

We present an analysis of the pointwise relationship between the reflectance of print and the surface topography of the paper before printing. We have measured the surface topography and reflectance of paper before and after printing in a sheet-fed pilot offset printing press. The 2D measurement maps have been aligned to obtain local print reflectance and surface topography values for every spatial position on the samples. In contrast to the various deterministic modeling approaches, which imply an a priori defined underlying mathematical model, we apply probabilistic analysis. Therefore we first estimate joint probability density functions (pdfs) of local topography and print reflectance using Gaussian Mixture Models (GMMs). From these pdfs we select paper regions with unusual properties, i.e. regions from the tails of the pdfs. These anomaly maps are analyzed for interrelations between the print reflectance and surface topography, its gradient

[1] Corresponding author, email: marja.mettanen@tut.fi

and local variance. The degree of interrelation is characterized by the mutual information (MI), a measure to quantify statistical dependence without making assumptions about the linear or non-linear nature of the regression dependence. The significance of the MI values is confirmed by simulation based statistical hypothesis testing. The objective is to offer answers to the question: How does the observation of an exceptional topography point on the paper surface change our information about whether the print quality attainable at that point will be exceptional or not? The results suggest that topography in combination with its local variance have the most prominent interrelation to small scale print anomalies. Furthermore it is shown that regions with abnormal topography have at least ten-fold higher probability to exhibit exceptionally high print reflectance, compared to randomly selected regions.

1 INTRODUCTION

Earlier work in the research of paper related print unevenness has focused on identifying overall paper properties, such as PPS roughness, air leakage porosity or formation index that would explain variations in print quality. These studies (e.g. [1–3]) analyzed the relationship between paper properties and print quality, also including parameters related to ink properties and to the printing process. Print quality was assessed with ink demand, print-through and evenness of the scanned reflectance of printed area [4], or with subjective quality rankings [5]. Regression models in which print quality was explained in terms of paper properties were identified. Extensive studies were also published on identifying and evaluating the ink transfer equations that would relate the amount of ink transferred to the paper with the characteristics of the paper and the printing process (e.g. [6–8]).

In more recent work 2D measurements of local paper properties have been increasingly employed as many small-scale print defects can directly be related to inhomogeneities in the paper structure. Statistically significant correlations have been established between spatially aligned 2D measurements of paper surface topography, formation and print quality (local gloss or print reflectance) [9–12]. These studies have focused on identifying deterministic relationships, usually linear ones, between local paper properties and local print characteristics.

In our work we will also examine the relationships between a local paper property, namely surface topography, and local print reflectance[1]. However, we do not employ deterministic models, but instead we analyze the probabilistic relationship. Our key approach is to identify 'abnormal' regions in the paper by analyzing the (joint) probability density functions (pdfs) of the measured properties. By 'abnormal regions' we mean paper regions that have very unlikely, i.e. extreme, properties compared to the typical statistical behaviour of the data. Such regions correspond to values in the tails of the pdfs. Having identified the 'abnormal' regions we examine the relationship between surface topography and print reflectance in these regions. These relationships are quantified using mutual information (MI), a measure for the mutual dependence between the variables in the pdf. We compute MI from Gaussian Mixture Model (GMM) estimates [14, 15] of the joint pdfs of the abnormal points, which gives more stable results than computing MI directly from histograms [16]. We also examine conditional probabilities to quantify how much more likely it is that a print defect occurs at a point of an exceptional topography than on the average, and study how much the answer will depend on the size of the exceptional topography area.

This paper is organized as follows. In Section 2 we introduce the measurements analyzed in this work and describe the alignment of the measured 2D maps. Section 3 introduces the statistical analysis methods that we apply to the image data, and it also proposes two approaches to test the statistical significance of the analyses. Results are presented in Section 4 and conclusions are drawn in Section 5.

2 MEASUREMENT DATA

2.1 Measurements

In this work we concentrate on analyzing the dependence between the reflectance measurements of printed paper and the surface topography of the paper before printing. The applied topography measurement method is based on photometric stereo and it closely resembles the one presented in [17]. It is a camera-based measurement that provides reflectance and topography maps from exactly the same area of the paper sample. The test areas of paper samples have been imaged in this study both before and after printing. We interpret the reflectance measurement of the printed paper so that dark areas correspond to normal print quality and the bright spots in the reflectance

[1] This is not a true reflectance measurement (as described in [13]) but rather a photographic image of the paper surface.

map correspond to local print defects with missing or inadequate ink transmission. In the surface topography presentation, dark shades of gray are used to denote pits and light shades denote surface elevations.

The measurement data analyzed in this work is from a printing test where 16 newspaper sheets with PPS roughness of 2.61 μm, 2.77 μm, 3.16 μm or 3.63 μm (4 sheets each) have been printed with a sheet-fed pilot offset printing press. Each of the 16 paper sheets contains two test areas relevant for this work, both printed with full tone cyan. One of the areas has been printed with normal 4-colour offset settings with all four printing units pressing the paper. The other area has been printed so that only the cyan printing unit is in contact with the paper and thus the back-trap phenomenon is eliminated. On one of the paper sheets, the normal cyan area has been discarded from the analysis because the sheet has wrinkled at the printed area. The final number of imaged areas is thus 31, containing 15 normal cyan areas and 16 non-back-trap areas. The size of each imaged area is 22.5 mm by 15 mm and the image size is 2268 by 1512 pixels. This results in a pixel size of 10 μm by 10 μm.

The analyzed surface topography maps have been high-pass filtered with wavelength limit 250 μm, which emphasizes the sharp pits and elevations on the surface. A local variance map and a map of the local gradients in the printing direction have been computed from the high-pass filtered topography and used in the analyses as well. This allows also other surface properties than height to explain the print quality.

2.2 Image alignment

Accurate alignment of the 2D measurements is a prerequisite for the probabilistic analysis. The printed reflectance measurement is, due to the measurement method [17], already exactly aligned with the printed topography map, and the same holds for the measurements of the unprinted paper. Thus it is sufficient to register and align either the reflectance or topography measurements acquired before and after printing. We register the unprinted and printed topography maps because they resemble each other more than the unprinted and printed reflectance measurements.

The image registration is based on point mapping [18] that is the primary approach to register images with random textures. A set of matching points is searched from the reference and target images (i.e., the unprinted and printed topography maps) using cross-correlation coefficient of the surroundings as the similarity measure of the matching points. Typical values of the local cross-correlation maxima are above $r = 0.8$ when registering the topography maps. The subpixel coordinates of the cross-correlation maxima are estimated by fitting a second order 2D polynomial to the surroundings of each cross-correlation peak. This provides the subpixel coordinates of the matching points. A global affine transformation [19] is fitted to the set of matching points and applied to the coordinates of the target image to overlay them with those of the reference image. Our registration is in two phases for accuracy, computational efficiency and robustness. The first phase estimates the translation only, and the second phase iteratively refines the transformation estimate, introducing also the rotation and shear deformation. When the selected affine transformation model is appropriate for the application, the transformation fitting error is less than 0.1 pixels [20]. The details on the image registration procedure have been presented in [20, 21].

The camera optics causes slight geometric distortion at the edges and corners of the images. As a result, the selected global affine transformation is not exactly the optimal way to warp the coordinates. The error that remains between the aligned coordinates may exceed one pixel in the corners of the image. To ensure accurate pointwise analysis of topography and print reflectance, only the parts of the images with less than half a pixel dislocation have been selected for the analysis. Still, the number of the pixels included on each of the 31 test areas is more than two million.

3 STATISTICAL ANALYSIS

After aligning the measurements, we analyze the dependence between the measured variables. We analyze probabilistic relationships instead of deterministic models because we do not want to restrict ourselves to an a-priori defined deterministic model between print reflectance and surface topography. In probabilistic analysis, we measure the interdependence of the variables based on their marginal, conditional and joint probability density functions (pdfs). Examples of pdf estimates for two variables are given in Figure 1. The *marginal pdf* of one variable is the 1-dimensional pdf calculated from the 2D pdf by integrating over the whole range of the other variable, Figure 1 (b-c). The *conditional pdf,* $f_{Y|x}(y|X = x)$, is the probability density of variable Y given a fixed value $X = x$, e.g. the print reflectance given that surface topography is −3.5 μm, Figure 1 (a,c). Such analysis reveals how much information we gain on the printed reflectance in a specified point by observing the value of the surface topography in that point.

Generally, a relatively small number of observations suffice to estimate reliably the pdfs of the variables in their normal value range. However, it is especially important to have reliable estimates for the tail regions of the pdfs because they represent the abnormal regions of paper we are interested in.

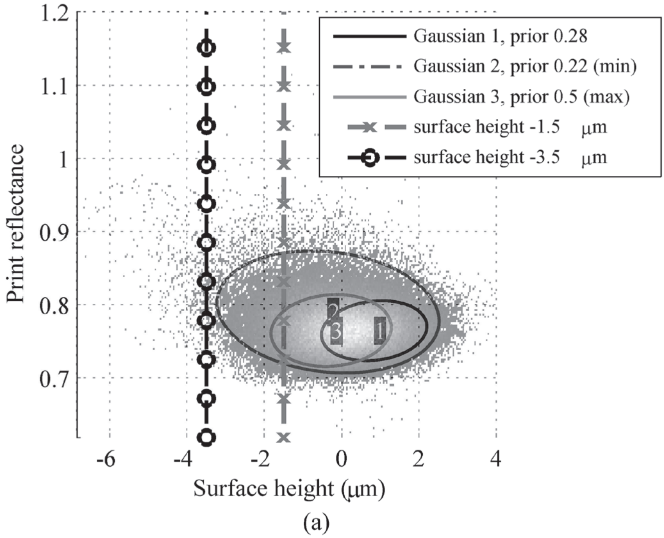

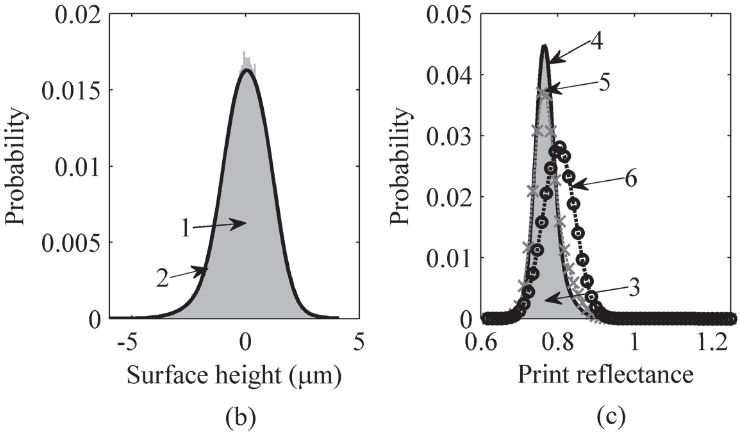

Figure 1. (a) Histogram-based and GMM-based joint pdf estimates of surface topography and print reflectance. The ellipses denote the 2σ equal probability contours of the components of the GMM. (b) Marginal pdf of surface topography (1: histogram-based, 2: GMM-based). (c) Marginal pdf of print reflectance (3: histogram-based, 4: GMM-based), and the conditional pdfs on condition that surface topography value is –1.5 μm or –3.5 μm (curves 5 and 6, respectively).

With image based measurements, we have huge amounts of data and thus we can obtain pdf estimates that describe reliably also the low-probability tail areas of the pdfs. Certain observed values can be classified as abnormal based on their falling into the tail area of the pdf. Thus we can analyze, how much information we have on the reflectance in a specified point given that the corresponding surface topography value has been deemed abnormal.

In this section, we first briefly introduce the GMM method by which we estimate the probability density functions. We study marginal and conditional pdfs and recognize the weak overall dependence between surface topography and print reflectance. Then we proceed to the selection of the abnormal points and study how they are located in the measurement area. As the first approach to verify the statistical significance of the analysis results, we present a method to test whether the abnormal points are spatially localized or just randomly and independently distributed in the plane. We then introduce the concept of mutual information (MI) to characterize the probabilistic dependence between two or more variables. Our second approach to verify the significance of the results consists of a comparison of the obtained MI values with the corresponding simulation results. The simulation is based on null hypothesis that print reflectance and surface topography are statistically independent. The last subsection provides more insight into the interpretation of the MI results by considering the probabilities of coincidences of abnormality in the measured variables.

3.1 Estimation of probability density functions

The joint probability density functions (pdfs) of the variables analyzed in this work differ clearly from Gaussian distributions. Thus they are estimated with Gaussian Mixture Models (GMMs) [14], known to describe complex multivariate pdfs with quite few parameters. A GMM is a weighted sum of N Gaussian distribution components. For a d-dimensional random variable $\mathbf{X}$ the pdf is described by GMM as

$$f(\boldsymbol{x}) = \sum_{i=1}^{N} c_i (2\pi)^{-d/2} \left(det(\boldsymbol{C}_i)\right)^{-1/2} exp\left[-\frac{1}{2}(\boldsymbol{x}-\boldsymbol{\mu}_i)^T \boldsymbol{C}_i^{-1}(\boldsymbol{x}-\boldsymbol{\mu}_i)\right]. \quad (1)$$

Only three types of parameters are needed for each Gaussian component: the weight of the component c_{i} (prior), mean vector $\boldsymbol{\mu}_{\mathrm{i}}$, and covariance matrix $\mathbf{C}_{\mathrm{i}}$. The parameters can be estimated by the expectation maximization (EM) algorithm [22]. We apply the algorithm described in [23] which – unlike the standard EM algorithm – is capable of selecting the number of mixture components without supervision. It is worth noting that the true probability distribution of the underlying random variable **X** is unknown, and thus the estimation procedure is initialized randomly and it searches the optimal parameter values iteratively. Two GMM models trained with the same data thus differ slightly from each other but both are appropriate estimates of the true pdf when the number of points used for the estimation is high enough. We always use more than a thousand data points to estimate a GMM, which produces very robust results.

Figure 1 (a) gives an example of a 2D joint pdf approximated as the joint histogram and modeled as a 3-component GMM. The marginal pdfs of the variables are shown by the discrete histogram presentations and continuous GMMs in Figure 1 (b-c). In Figure 1 (c), two conditional pdfs of print reflectance are exemplified, given that the surface topography value is fixed either at −1.5 µm or at −3.5 µm. In the former case, the conditional and marginal pdfs of print reflectance closely resemble each other, while the latter conditional pdf clearly deviates from the marginal pdf. This illustrates the fact that the statistical dependence between print reflectance and the unprinted surface topography is considerably stronger at the markedly low values of surface topography (−3.5 µm) than at the relatively typical topography values (−1.5 µm).

3.2 Selection of points based on abnormality

The overall dependence between surface topography and print reflectance is weak, as exemplified in Figure 1. This means that predicting the print reflectance in a specified point by measuring the surface topography in that point is highly uncertain in the general case: very little information in addition to that provided by the marginal pdf is gained. We therefore proceed to identifying and examining the abnormal points of the measured maps. The hypothesis is that the dependences are much more significant at the tail areas of the distributions.

3.2.1 Construction of the mask

A binary mask is constructed to select the abnormal points from the measurement data. The mask can be formed based on the joint pdf of the measured variables, or based on the extremeness of the values of single variables. Figure 2 exemplifies the mask identification procedure using the joint pdf of unprinted surface topography and print reflectance as a basis for the mask. The joint pdf is visualized by the joint histogram, and the line on top of the histogram denotes the mask criterion boundary. The mask selects the points outside the boundary, i.e. the points that correspond to the least likely

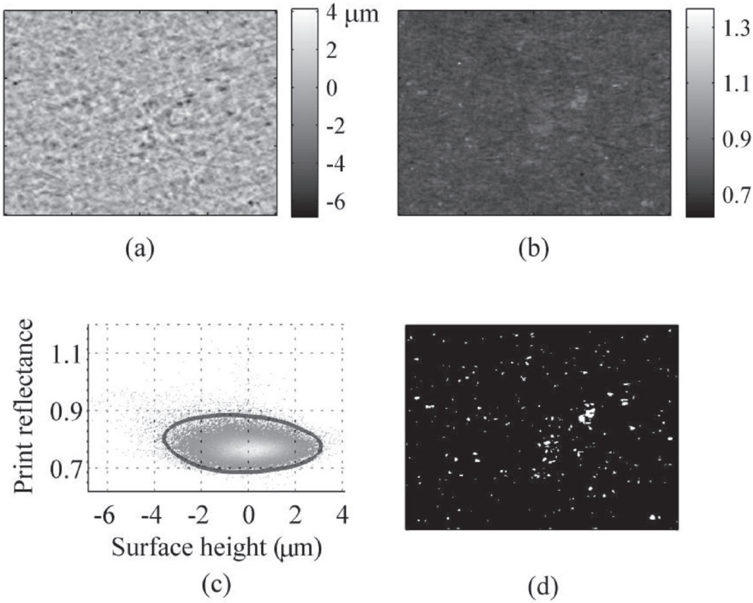

Figure 2. (a) Unprinted high-pass filtered surface topography and (b) print reflectance (reflected intensity in arbitrary units) on a 4 mm by 3 mm selection of a full tone cyan printing area. (c) Joint histogram of the variables together with the probability thresholding limit, $C(p)$ (gray curve), where $p = 1.5$ %. (d) The resulting mask that shows by white the 1.5 % of pixels with the most unlikely combinations of topography and print reflectance.

p percent of the combinations of surface height and print reflectance. These points of the mask are given a value 1 while the rest of the mask assumes value 0. Figure 2 (d) shows the $p = 1.5$ % of pixels that have the lowest values in the joint pdf, Figure 2 (c).

Mathematically, denoting the pdf of the (vector) variable $\mathbf{X}$ as $f(\mathbf{X})$, the condition for an observation $\mathbf{x}$ at location i to be abnormal to degree p is

$$f(x) < C(p), \tag{2}$$

where the relationship between C and p is determined through

$$p = p(C) = \int_{f(x)<C} f(x)\, dx. \tag{3}$$

The mask indicates those locations i that satisfy the above condition at the

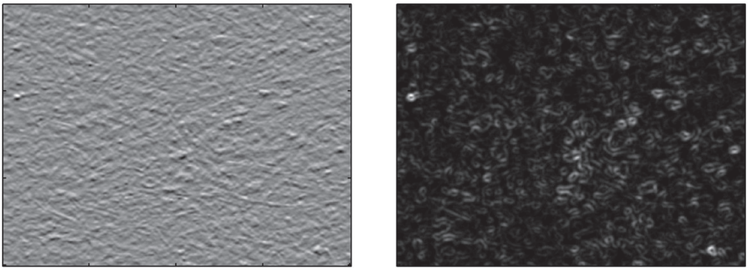

(a) (b)

Figure 3. (a) Gradient and (b) local variance maps of the surface topography shown in Figure 2 (a). The gradient has been computed in the printing direction, i.e. y-direction. Both maps have been normalized to unit variance and thus the color bars are not shown.

chosen degree of abnormality, p. In other words, the selected points are responsible for the percentile p of the distribution of $\mathbf{X}$. In the case shown in Figure 2, the random variable $\mathbf{X}$ is 2-dimensional, containing the observations of both surface topography and print reflectance.

We evaluate the relationship between surface topography and print reflectance in two setups: in 'forward' and 'backward' analysis. In the backward analysis we select regions with 'abnormal print', using the tail of the marginal pdf of print reflectance, and examine whether the topography might be responsible for these print defects. In forward analysis, we test how well the various selections of surface property characteristics are able to predict missing ink. The mask regions are selected according to paper surface properties: surface topography, its gradient and its local variance. We employ both the marginal and joint pdfs of the surface properties to select the abnormal points from the topography map, and then we examine the interrelation of these points with the local print reflectance. Figure 3 presents the gradient and variance maps corresponding to the surface topography shown in Figure 2 (a).

The mask construction methods that directly select the mask points from the tail areas of the pdfs, as discussed above, operate over the whole image area at once. We have additionally examined in the forward analysis a two-step mask construction procedure in which the selected areas are locally refined. This procedure is aimed to find regions with low topography values that additionally have large local variation in topography.

Step 1:

a. Select a relatively small number, K, of the lowest values of the surface topography map.
b. Assign a label to each connected group of pixels found. This produces a 'seed mask' with typically 100–200 labeled objects.

Step 2: Repeat for each seed object

c. Set a window of size d by d pixels around the center of the seed object.
d. Select a percentage q of the highest local variance values inside the window.
e. Assign a label to each connected group of pixels found in the local window. This produces a local d by d mask with typically 1–5 labeled objects.
f. Augment the seed object by the all the local labeled objects that have overlap with the seed object.

The result of the second stage is an augmented topography mask that takes into account the shape of the surroundings of the topography pits. We have used the following parameters in the algorithm: $K = 1000$, $K = 1500$ and $K = 2000$; $d = 35$; $q = 5$ %.

Unlike the other masks, a fixed mask percentage is not applied in this technique. Instead, the number of pixels selected by the mask depends on the content of the image and on the parameters defined above. We have applied very low values of K in the seed masks, which produces low mask percentages, typically 0.2 % . . . 0.5 %. The choice of small K was made because the objective was to produce masks that differ clearly from the other forward masks. In addition, the labeling and processing of the seed objects becomes computationally demanding when the number of seeds increases. Table 1 summarizes the masks used in the analysis.

3.2.2 Spatial correlation of mask points

Studying the coincidence of abnormality at single pixel level is rather a limited perspective. We include the spatial aspect of abnormalities as follows. After constructing the mask, we examine how the masked points are distributed in the plane by counting the number of 1's in the mask inside a sliding window. The statistical significance of the spatial extent of mask point areas is evaluated by comparing the result of the sliding summation to the null hypothesis of uniformly and independently distributed mask points. If the null hypothesis is true, the summation in the sliding window produces binomial distributed numbers. As the average mask coverage is small, it is

Table 1. Summary of masks.

Analysis	*Mask name*	*Points selected according to*	*Mask percentages*
Forward	Topo	lowest values of unprinted topography	0.2 % . . . 1.5 %
Forward	TGV	most unlikely combinations of topography, its (y-)gradient and its variance	0.2 % . . . 1.5 %
Forward	LocalVar	a low percentage of the lowest topography spots with local refining to take into account the variance of surface topography values around the selected pits	0.2 % . . .0.5 %
Backward	Refl.	highest values of print reflectance	0.2 % . . . 1.5 %
Overall	Random	uniformly and randomly distributed points	0.2 % . . . 1.5 %

particularly efficient to test the null hypothesis by studying the distribution of the *maximum* number of points within the sliding window.

The null hypothesis can be simulated by repeatedly drawing M samples from a binomial distribution with parameters n and p, where n denotes the size (in pixels) of the sliding window and p is the mask coverage. We denote the samples as $N \sim \mathrm{bin}(n,p)$. The number of samples, M, equals to the number of pixels in the image divided by n, i.e. the number of independent summation results obtainable in the image area. The histogram in Figure 4 (a) presents the distribution of $M = 10785$ samples from a binomial distribution with parameters $n = 225$ and $p = 0.015$, and implies that if the mask points were uniformly and independently distributed, a sliding 15 by 15 (i.e. 225) pixel window would almost always contain 10 mask points or less. The maximum of the M-sample set is recorded; the maximum in the simulation run shown in Figure 4 (a) was 12. To obtain a histogram estimate of the distribution of the *maximum* number of 1's in the mask inside a sliding window when the null hypothesis is true, we could repeat the experiment many times, each time recording the maximum value from the M-sample set. However, there is an analytical way. If the mask point positions are correlated, there will be more samples of exceptionally high density of points (inside a window) than according to the null hypothesis. Hence we choose as our decision variable the maximum of N among the M observations and call it $N_{\max}$. The probability that the random variable $N_{\max}$ (in M observations) takes a given value

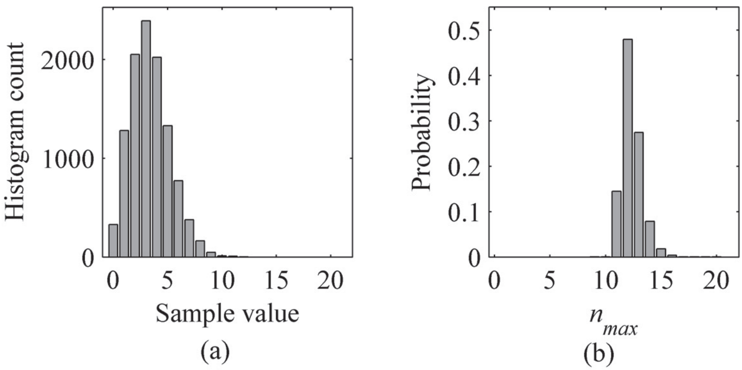

Figure 4. (a) Histogram of 10785 binomially (bin(n,p)) distributed random numbers with parameters n = 225 and p = 0.015. (b) Probability of the maxima of drawing 10785 samples from bin(225,0.015).

$n_{\max}$, $P_{\max}(N_{\max} = n_{\max})$, can be calculated with standard order statistics. Figure 4 (b) illustrates such probability $P_{\max}$ as a function of $n_{\max}$.

The idea behind this test is to show that the mask regions found by our procedures are much larger than for random masks. This indicates that the selected abnormal points are not uniformly placed but spatially correlated, i.e. they in fact represent regions of abnormal paper properties. The spatial correlation of the points of the mask under testing is statistically significant at points where the sliding summation result of the mask exceeds a chosen percentile, e.g. 99%, of $P_{\max}$.

We apply the simulation results in Section 4 and show that in our masks the number of 1's inside a sliding window exceeds the maxima of the binomial distributed numbers and thus our masks are not random.

3.3 Analysis of dependence through mutual information

3.3.1 Mutual information

Mutual information (MI) characterizes the interdependence of any two random variables, whatever the functional form of their joint pdf may be, and without making assumptions about the linear or nonlinear nature of their regression dependence. MI specifies how much the uncertainty about one variable is reduced by knowing the value of the other variable: it is a measure of how much information a variable carries about another variable. MI is symmetric and always non-negative – it reaches the value of zero if and only if the variables are statistically independent. MI is calculated between the measured variables based on the pdf estimate. We use the parametric GMM presentation of the joint pdf instead of histogram because the former produces robust MI estimates whereas the histogram based MI depends heavily on the number of histogram bins [16]. Let us denote by **X** and **Y** the (possibly multidimensional) random variables. Let the joint pdf be $f(\mathbf{x},\mathbf{y})$ and the marginal pdfs of **X** and **Y** $f_X(\mathbf{x})$ and $f_Y(\mathbf{y})$, respectively. The MI between **X** and **Y**, $I(\mathbf{X};\mathbf{Y})$, is defined as [15]

$$I(\boldsymbol{X};\boldsymbol{Y}) = \int_Y \int_X f(\boldsymbol{x},\boldsymbol{y}) log\left(\frac{f(x,y)}{f_X(x) f_Y(y)}\right) d\boldsymbol{x}\, d\boldsymbol{y}. \quad (4)$$

If the logarithm is of base e, the unit of MI is nat, and with base 2 logarithm the unit is bit.

By the concept of mutual information, it is possible to examine any statistical dependences, without restricting the analysis to the Gaussian statistics as the standard correlation and R-squared analyses do. However, the interpretation of MI is less intuitive. In the case of jointly Gaussian distributions, the dependence between two variables, X and Y, is linear, and MI reveals information identical to the coefficient of determination of linear regression, R^2. For joint Gaussian pdfs, MI is related to this familiar R-squared concept by [24]

$$I(X;Y) = -1/2 * \log(1 - R^2) \quad (5)$$

The same can be generalized to the Gaussian joint distributions of more than two variables by using the covariance matrix instead of a scalar correlation coefficient.

In a typical data analysis task the distributions are not Gaussian, and the above reasoning is inadequate. In practice, the absolute values of MI may not be as important as the maximization of MI with respect to certain criteria. This is the case, for instance, in various image registration applications where the objective in optimizing the image transformation parameters is to maximize the mutual information between the pair of images [25, 26]. In our analyses, the absolute MI values are also of less importance. We measure the MI between print reflectance and the topography-related variables and search for a topography-based strategy of selecting the abnormal points that maximizes the MI. Interpretations for the results are searched through comparisons and simulations, as described in the rest of this section.

3.3.2 Statistical significance of mutual information

We estimate MI from data sets selected by the masks described in Section 3.2.1. Because MI is by definition larger or equal to zero, the MI estimate from a finite data set is always larger than zero even if the sampled variables were statistically independent. To assess the statistical significance of the MI between random variables **X** and **Y**, we test by simulations, how estimated MIs are distributed when variables are statistically independent and the data set is of finite size.

The first idea to simulate statistically independent data sets might be to use white noise. However, when the masks are set up according to the true data, the simulated data must have spatial correlations identical to the ones in true data of each of the individual variables. Thus we need a procedure to make the topography and print reflectance maps statistically independent while maintaining their internal spatial structure. This can be achieved by randomizing one of the maps. We have chosen rather arbitrarily the topography map to be randomized.

The key idea in the randomization of the topography map is that the spectrum of the random map is kept identical to the spectrum of the original topography map, and hence the spatial autocorrelation of the data is kept identical as well. This is achieved through manipulation in the Fourier domain. The high-pass filtered surface topography map is first transformed into the Fourier domain by 2D Fast Fourier Transform (FFT). Then the phases at each frequency are chosen as randomly and uniformly distributed values between 0 and 2π while keeping the amplitude unchanged. Finally the 2D inverse FFT of the modified Fourier transform produces a topography map whose variance and spectrum are identical to those of the original map but which is uncorrelated with the original map. We refer to the resulting image as random-phase topography. Figure 5 presents a comparison of the original and simulated topography maps, their spectra and the corresponding pdfs. The original and simulated pdfs differ slightly because the original pdf was not Gaussian which would be a prerequisite to preserve the exact pdf. The slight differences between the original and simulated spectra are caused by the finite size of the image: edge effects are not simulated in the random phase spectrum.

Figure 6 gives an example of simulated and true MI values between surface topography and print reflectance. Both the true and simulated cases employ the true print reflectance map and select the data points using a locally refined topography mask (LocalVar mask with $p = 0.3$ %), but the simulation uses random-phase topography images in the place of the true topography measurement. Both sets of results have variance larger than zero but the MIs

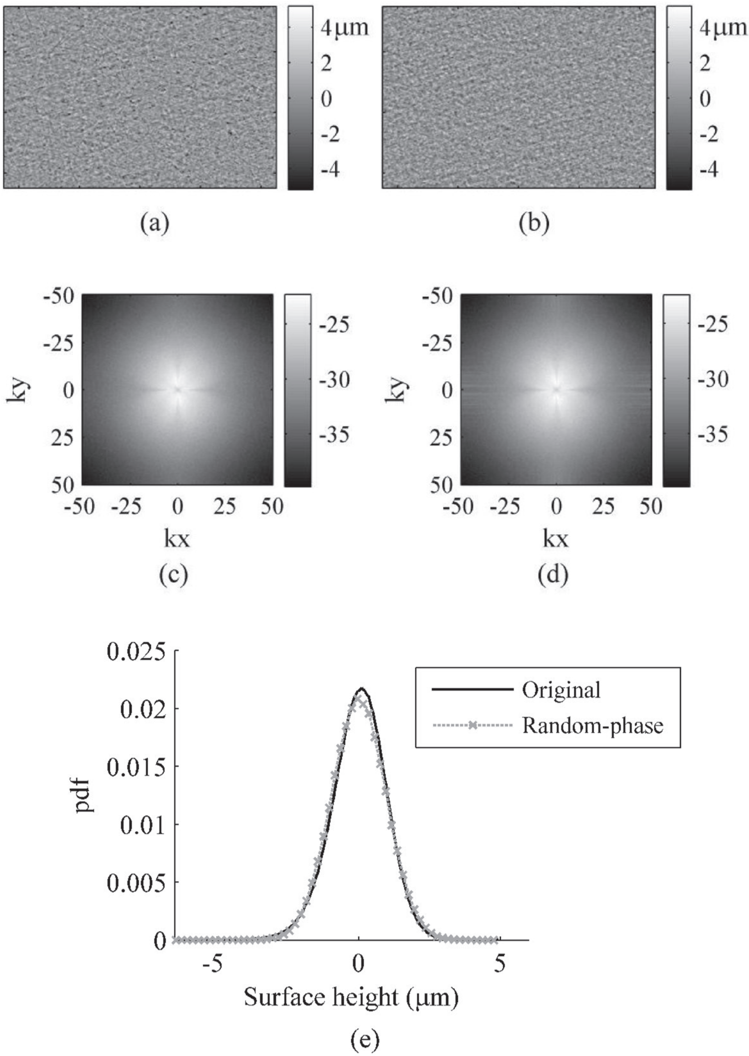

Figure 5. Simulation of topography by randomizing the phase information. (a) Original surface topography on a 9 mm by 6 mm selection, (b) corresponding random-phase topography, (c) logarithm of the 2D spectrum of the original topography, (d) logarithm of the 2D spectrum of the random-phase topography, (e) marginal pdfs of the original and random-phase topography images.

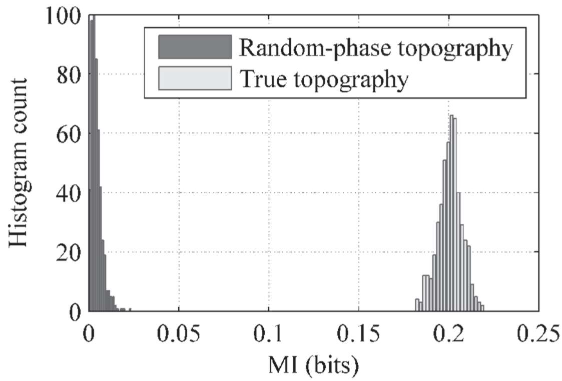

Figure 6. Histogram of 500 MI values computed between print reflectance and simulated topography and comparison with 500 repetitions of MI computation using the true data from one of the non-back-trap cyan samples.

computed from true data are always much higher than the simulated MIs. The differences in MI between repeated calculations are caused by three factors. Firstly, since we are estimating the pdfs by GMM using a different random initialization each time, the GMM estimates differ slightly from each other even if the input data stays exactly the same. Secondly, the numerical integration applied in the MI computation causes minor deviation to the results. Thirdly, in the simulation, we generate a new random-phase topography data at each simulation experiment.

3.4 Coincidence of abnormalities

As the final analysis method, we examine the coincidence of abnormalities in the measurements. We classify the observations of topography and print reflectance into normal or abnormal classes individually – with their marginal probabilities – and then compute the probabilities of coincidences of abnormality, p($y \neq$ normal | $x \neq$ normal). This resembles the technique used in [9]. Specifically, we measure the probability of having a print defect in a spot that has been deemed abnormal based on its surface topography. We also examine the dependence of the results on the size of the exceptional topography spot.

We do not have subjective evaluations or other references to classify the values of the print reflectance map as normal or abnormal. Therefore masking is based on the selected degree of abnormality, i.e., the selected percentile of the pdf that determines where the 'normal' part of the pdf turns into the 'abnormal' tail. Various mask percentages are tested. We apply the same mask percentage to both the print reflectance map and the surface topography map, and then examine the overlap of the masks. If the occurrence of an abnormality in the print reflectance does not depend on the classification (normal/abnormal) of the corresponding spot in the surface topography map, the expected overlap of the masks equals the selected mask percentage. The results presented in Section 4 show that the overlap percentages are considerably larger than that. This will provide a new insight into the interpretation of the MI results as well.

4 RESULTS

Masks with abnormality degree, p, varied between 0.2 % and 1.5 % have been generated for the whole set of images. The masks indicate the p percent most abnormal points of the variables and their combinations according to the 'forward' and 'backward' approaches introduced in Section 3.2.1. The backward approach applies a mask that indicates the highest values of the print reflectance map (Refl. mask) and the forward approach applies three topography-based masks (Topo, TGV, and LocalVar masks) as listed in Table 1. In addition, we have used a random mask in which the number of points specified by p is distributed independently and uniformly on the image area. This corresponds to modeling the overall dependence between print reflectance and unprinted topography, without classifying the observations into normal or abnormal categories.

In this section, we first verify the spatial correlation of the mask points by comparing the masks with the null hypothesis of randomly and independently distributed mask points, as described in Section 3.2.2. Then, for each mask, we estimate the joint pdf of the variables in the points indicated by the mask, and calculate the mutual information from the pdf. The statistical significance of the MI results is evaluated by comparing the results with simulations that use random-phase surface topography instead of the original aligned topography map, as described in Section 3.3.2. Finally, we study the overlap of the forward and backward masks and show that observing an exceptional value in the surface topography map provides useful information for predicting the occurrence of a print defect in that point.

4.1 Spatial correlation of mask points

We test whether the positions of mask points in the image are correlated or not, the null hypothesis being that no correlation exists. Let us study a window of $\sqrt{n}$ by $\sqrt{n}$ pixels within the image. If the mask point positions are not correlated, then the number of mask points within such window is binomially distributed $N \sim \text{bin}(n, p)$, where p is the proportion of masked points in all the points (i.e. the mask percentage). If the image size is $\sqrt{m}$ by $\sqrt{m}$ pixels we may generate $M = m/n$ independent samples of N. If the mask point positions are correlated, there will be more samples of exceptionally high density of points and exceptionally low density of mask points than according to the null hypothesis. Hence we choose as our decision variable the maximum of N among the M observation and call it N_{max}.

As noted in Section 3.2.2, the probability that N_{max} (in M observations) takes a given value n_{max}, $P_{max}(N_{max} = n_{max})$, can be calculated with standard order statistics. The probability in the case $n = 225$, $p = 0.015$ and $M = 10785$, corresponding to the mask parameters studied in Figure 4 in Section 3.2.2, is shown in Figure 7 (a). The probability that N_{max} exceeds the value $n_{max} = 17$ is 0.001. Figure 7 (b) gives a typical example of observed distribution of number of mask points per 15 by 15 pixel windows with 10785 independent observations in total. The maximum of these is over 100. Hence the null hypothesis is rejected on a confidence level of 0.001 and we conclude that the positions of mask points in the images are correlated.

For all paper samples, the Topo, TGV and Refl. masks with 5 mask percentages varying between 0.2 % and 1.5 % have been analyzed by the sliding summation technique using window sizes from 10 by 10 pixels to 30 by 30

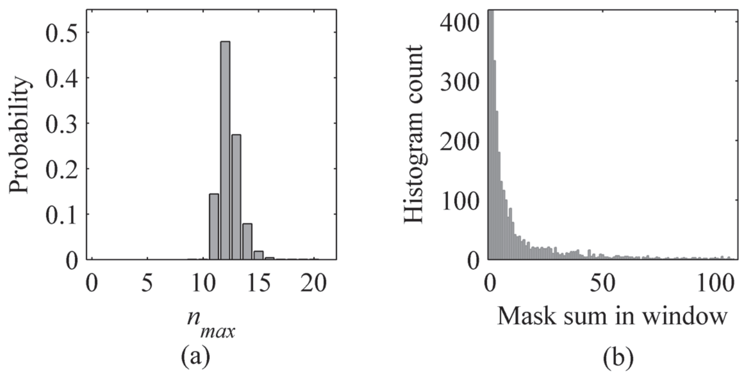

Figure 7. (a) Probability of the maxima of random variables from binomial distribution bin(255, 0.015). (b) Histogram of the 10785 sums of a 1.5 % TGV mask inside a sliding window of size 15 by 15 (255) pixels. The axes in (b) have been zoomed for visualization: the highest peak was 8208 and the last non-zero bin was 181.

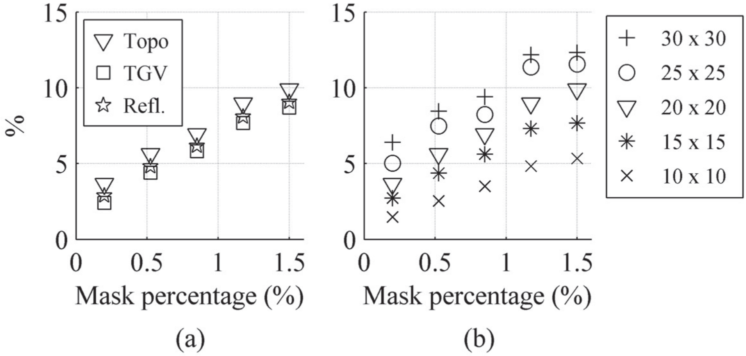

Figure 8. The proportion of the mask pixels that are to a very high probability spatially concentrated. (a) Topo, TGV and Refl. masks with window size 20 by 20 pixels, (b) Effect of window size demonstrated with the Topo mask. In (b), the reference binomial distribution corresponding to a marker has parameters *n* and *p*, where *n* is denoted by the marker type and *p* is the location of the marker on the x-axis.

pixels. Each time the histogram of the sliding summation results has been compared with the corresponding maxima histogram obtained from the repeated binomial distribution sampling. We have counted how large proportion of the independent sliding summation results exceeds the 99 % percentile of the maxima distribution such as that shown in Figure 7 (a). This is a measure for the proportion of mask pixels that is to a very high probability spatially concentrated. Figure 8 (a) presents the results for the three mask types with the window size fixed to 20 by 20 pixels. The local concentrations of the mask points are slightly more frequent in the Topo mask than in TGV and Refl. masks. Figure 8 (b) uses the Topo mask again to illustrate the effect of the sliding window size on the results. In conclusion, Figure 8 confirms that, independent of the selected mask percentage and type, there are always numerous locations in the mask where the local sum of the mask points exceeds the value that it would most likely maximally have if the mask points were randomly and independently distributed. The proportion of the significantly spatially concentrated mask points increases with the mask percentage.

4.2 Mutual information and its significance

With each mask, we have estimated by GMM the joint pdf of the masked points of the four maps: print reflectance (R), surface topography (T), the gradient of surface topography (G), and the local variance of surface topography (V). This joint pdf estimate is used to compute the mutual information between print reflectance and the topography-related variables and their combinations. From all possible combinations of datasets we report the results for the four combinations that contain reflectance and topography: RT, RTG, RTV and RTGV. It is thus possible to assess whether the gradient of the surface is a better predictor of print reflectance than the local variance of the surface topography, or vice versa.

To assess the statistical significance of the MI results computed based on the measurements, the corresponding MI values have been computed using simulated random-phase surface topography data together with the true reflectance measurements. In this analysis, the simulated topography map replaces the true topography before the gradient and variance maps are computed. The simulated topography map thus preserves its relationship with the gradient and variance maps like the original topography map. As described in Section 3.3.2, the simulation also preserves the spatial correlations of the original topography map, as well as the marginal pdf. When the simulated topography data is used in GMM estimation and MI computation together with the original reflectance map, the dependences are very weak because the topography is random with respect to the reflectance. The simulated case thus serves as a reference and indicates the level of MI attainable even with random data when the sample size is finite.

The smallest masks select 0.2 % of the points of the measurement maps (that is approximately 5000 data points) while the largest mask selects 1.5 %. The mask percentage slightly affects the MI values but the effect depends on the type of mask used. The results of the MI analysis are reported in Table 2 for the non-back-trap samples and in Table 3 for the normal samples. Comparison of the values shows that the interdependence between topography and print reflectance is stronger in the samples printed without back-trap conditions than with normal printing conditions. This seems reasonable since back-trap related print unevenness is also linked to paper properties like formation or porosity variations [27] which are not related to small-scale topography variations.

The MI values given in the tables are the average results of the 16 non-back-trap or 15 normal samples. The tables report the lowest and highest mask percentages used, and the MI results obtained with 0.3 . . . 1.2 % masks fall between these values. The standard deviations corresponding to the MI averages are not given in the tables but Figures 9 and 10 illustrate the deviation in the form of 95 % confidence limits.

Figure 9 shows a graphical view of the 'forward' analysis results with 0.37 % masks, and Figure 10 respectively the 'backward' analysis results with

Table 2. Average mutual information between topography characteristics and print reflectance for the 16 non-back-trap Cyan samples in forward and backward analyses, and overall (using the random mask). (*) Mask based on random-phase topography and applied to the same random-phase topography with true reflectance data. (**) Mask based on reflectance and applied to the same reflectance with random-phase topography. (***) Random mask applied to true reflectance and random-phase topography.

	MI (bits) with p = 0.2 %				*MI (bits) with p = 1.5 %*			
Mask	*RT*	*RTG*	*RTV*	*RTGV*	*RT*	*RTG*	*RTV*	*RTGV*
Forward								
LocalVar	0.27	0.33	0.34	0.39	–	–	–	–
TGV	0.25	0.31	0.30	0.37	0.17	0.20	0.22	0.25
Topo	0.06	0.08	0.10	0.11	0.09	0.12	0.14	0.15
RandPhase (*)	0.006	0.04	0.03	0.07	0.007	0.03	0.02	0.06
Backward								
Refl.	0.06	0.12	0.15	0.25	0.04	0.10	0.13	0.20
Refl.+RP (**)	0.01	0.06	0.08	0.16	0.003	0.04	0.06	0.12
Overall								
Random	0.04	0.07	0.10	0.12	0.03	0.06	0.09	0.11
Random+RP (***)	0.001	0.02	0.02	0.05	0.001	0.01	0.02	0.04

Table 3. Average mutual information between topography characteristics and print reflectance for the 15 normal Cyan samples in forward and backward analyses, and overall (using the random mask). (*) – (***): see Table 2.

	MI (bits) with p = 0.2 %				*MI (bits) with p = 1.5 %*			
Mask	*RT*	*RTG*	*RTV*	*RTGV*	*RT*	*RTG*	*RTV*	*RTGV*
Forward								
LocalVar	0.20	0.28	0.27	0.34	–	–	–	–
TGV	0.17	0.25	0.23	0.32	0.11	0.15	0.16	0.19
Topo	0.08	0.10	0.13	0.14	0.08	0.12	0.14	0.15
RandPhase (*)	0.01	0.04	0.03	0.06	0.006	0.02	0.02	0.04
Backward								
Refl.	0.03	0.09	0.12	0.21	0.02	0.08	0.10	0.18
Refl.+RP (**)	0.01	0.06	0.08	0.16	0.003	0.04	0.06	0.12
Overall								
Random	0.02	0.04	0.06	0.08	0.02	0.04	0.07	0.08
Random+RP (***)	0.002	0.02	0.02	0.05	0.001	0.02	0.01	0.03

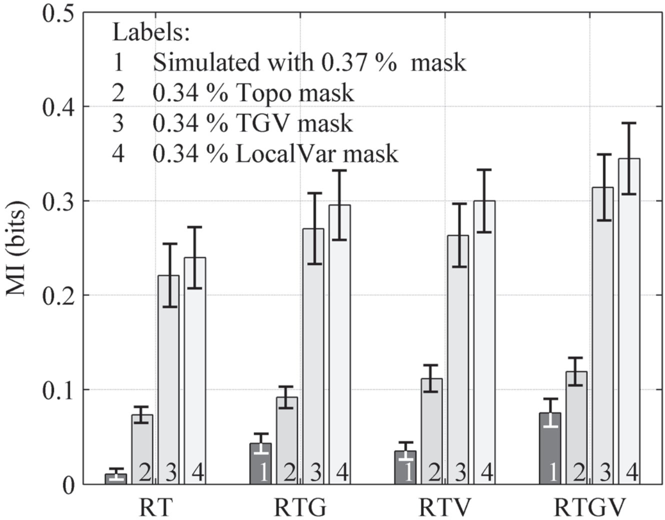

Figure 9. Comparison of MI in true topography-based masks and random-phase simulations for non-back-trap Cyan samples. Mutual information has been evaluated between the combinations of variables denoted on the horizontal axis. The whiskers at the end of the bars indicate the 95% confidence limits among the 16 samples.

the same mask percentage. The labeled bars in Figures 9 and 10 correspond to the masks listed in Tables 2 and 3. 'Forward' refers to the fact that abnormal points are identified based on paper surface properties that may give a prediction for the print result. 'Backward' means that the abnormal regions are identified from the print, which may be used to analyze the print defects. The overall mutual information results, computed without the identification of any abnormalities and given at the bottom of Tables 2 and 3, have not been plotted but they can be compared in the tables with the corresponding simulated results that use random-phase topography in the place of the true topography. The comparison shows that even though the overall dependence between surface topography and print reflectance is weak, it is consistently higher than the MI computed from random data.

According to Figure 9, the highest MI results are obtained by selecting the points by the locally refined topography mask that accounts for the variance in the surroundings of the selected topography pits (LocalVar mask). This masking strategy seems to be best suited to select regions in which the paper surface properties and print reflectance have significant statistical dependence. The mask based on the joint distribution of the three topography-

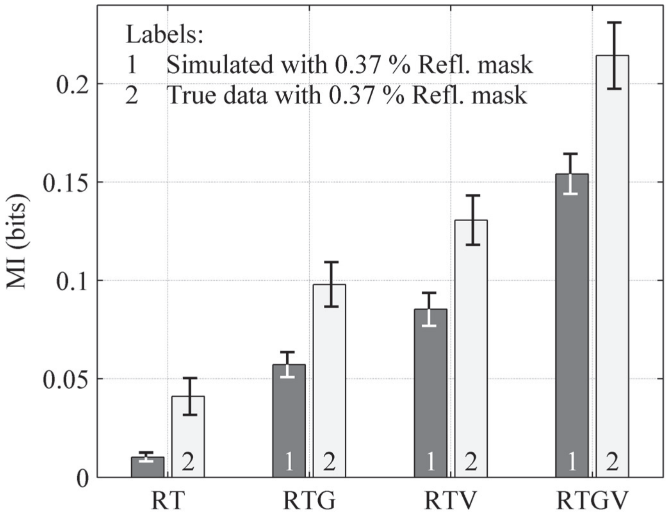

Figure 10. MI computed using true data from non-back-trap Cyan samples or a data set where the topography map has been replaced by random-phase topography. Both cases use a reflectance-based mask with $p = 0.37\%$. Mutual information has been evaluated between the combinations of variables denoted on the horizontal axis. The whiskers at the end of the bars indicate the 95% confidence limits among the 16 samples.

related variables (TGV mask) provides the second highest mutual information between the print reflectance and the explanatory variables. Comparison between TGV mask and Topo mask shows that surface topography, its gradient and local variance together reveal more interrelation between topography and reflectance than the topography map alone.

Mutual information between a set of variables can only increase or stay the same when the number of variables increases, because a new variable introduced in the joint pdf model can never reduce the dependences that have already been described by the model. Therefore the MI values – also the simulated ones – presented in Figures 9 and 10 increase from left to right, when the RT combination is switched to RTG or RTV, and further when proceeding to the 4-variable combination, RTGV. As the simulated values also increase, it is justified to assess how the MI develops in the variable combinations and masking strategies with respect to the simulated MI (the dark gray bars). Based on this comparison between the true data-based MI and the respective simulated results, MI is higher in the RTV combination than in the RTG combination in the backward mask and all forward masks, except the TGV mask. This implies that the local variance of surface topography may be a slightly better predictor of the print reflectance than the gradient of topography. Comparing the 3-variable and 4-variable combinations in the forward case reveals that MI is not significantly higher in the combination of all the four variables than in a combination of three variables where either the gradient or local variance of the surface topography has been excluded. In the backward analysis the fourth variable introduces some new information. This means that, for the prediction of print reflectance in the abnormal points of surface topography, the information between V and G is redundant, but when explaining the observed print anomalies by the topography characteristics, both the gradient and the variance carry useful information.

Finally, Figures 9 and 10 show that the dependence between surface topography properties and print reflectance is, on average, weaker in the print defect spots than in the spots of abnormal surface topography, because print defects are also caused by other paper properties than surface topography. However, identifying the abnormal topography points does facilitate the prediction of print reflectance.

4.3 Coincidence of abnormalities

The coincidences of the ‘forward’ masks with the ‘backward’ masks have been evaluated to measure the probability of observing an abnormally high value in the print reflectance map on condition that the surface topography in that point has been classified abnormal. The forward masks are the Topo, TGV and LocalVar masks that were used in the MI analyses as well, and the backward mask is the one that selects points of exceptionally high print reflectance. The coincidence analysis always applies the same mask percentage, p, for the forward and backward masks, studying the range from $p = 0.2$ % to $p = 1.5$ %.

The typical overlap of topography abnormalities with the points of unusually high print reflectance varies from 7 % to 12 % in the normally printed cyan samples and from 10 % to 18 % in the non-back-trap cyan samples. The Topo mask produces slightly higher overlaps than the LocalVar or TGV masks. The overlap percentages in all the cases are considerably larger than the probability for an accidental coincidence of the masks which equals p. As the mask percentage is increased, both the accidental and the realized overlaps of the topography and print reflectance abnormalities increase, but within the low mask percentages studied in this work, the latter increases considerably faster (as a function of p) than p itself. This means that the increase in the overlap is a result of true coincidence of abnormal regions in surface topography and print reflectance.

The forward masks have also been divided into sub-masks that only contain objects (connected group of pixels) of specified sizes, and their coincidence with the reflectance mask has been measured as the proportion of overlapping pixels. This reveals, as a function of the size of the exceptional topography area, the probability of observing an unusually high print reflectance on condition that the topography shows abnormal behavior.

Figure 11 presents the overlap results, averaged over the 16 non-back-trap samples within each mask type. For Topo and TGV masks, the smallest and largest mask percentages are presented, Figure 11 (a-d). In the locally refined topography masks the range of mask percentages is so narrow ($p = 0.2$ % . . . 0.5 %) that one diagram represents the results sufficiently. In the averaging between the paper samples, the overlaps in each size category have been weighted by the number of (the specified size) objects found in each sample. The variance of the overlap results among the paper samples is high in the size categories where the number of objects is relatively low. However, the results clearly show that, also inside the size categories, the surface topography anomalies coincide with print defects with a considerably higher probability than the accidental probability, p.

The results presented in Figure 11 cover the range of overlaps detected with the various mask construction techniques and mask percentages. The regions selected by the Topo mask show increasing overlap with the reflectance mask when the size of the abnormal topography regions increase, as illustrated in Figure 11 (a,b). With the TGV masks this tendency is not as strong as with Topo masks. The average overlap between the TGV mask regions and reflectance mask remains between approximately 10 % and 20 % over the range of object size categories in Figure 11 (d) where $p = 1.5$ %. At the lowest mask percentage ($p = 0.2$ %), Figure 11 (c), the TGV mask selections do not coincide with the brightest print reflectance points so well. Figures 11 (e) shows that abnormal topography regions of small size have particularly high overlap with the mask of print defects, if these topography regions are selected by the LocalVar mask. The differences in the results between the mask types are addressed to the fundamentally different methods of constructing the masks. The TGV and LocalVar masks tend to select larger individual regions of the topography map than the Topo mask because the former are based on the properties of the surroundings of the topography depressions, and not only the topography values as such. Overall, this reason reduces the overlap of the TGV and LocalVar masks with the corresponding reflectance mask.

Topo mask reaches the largest overlap with the print defects, whereas

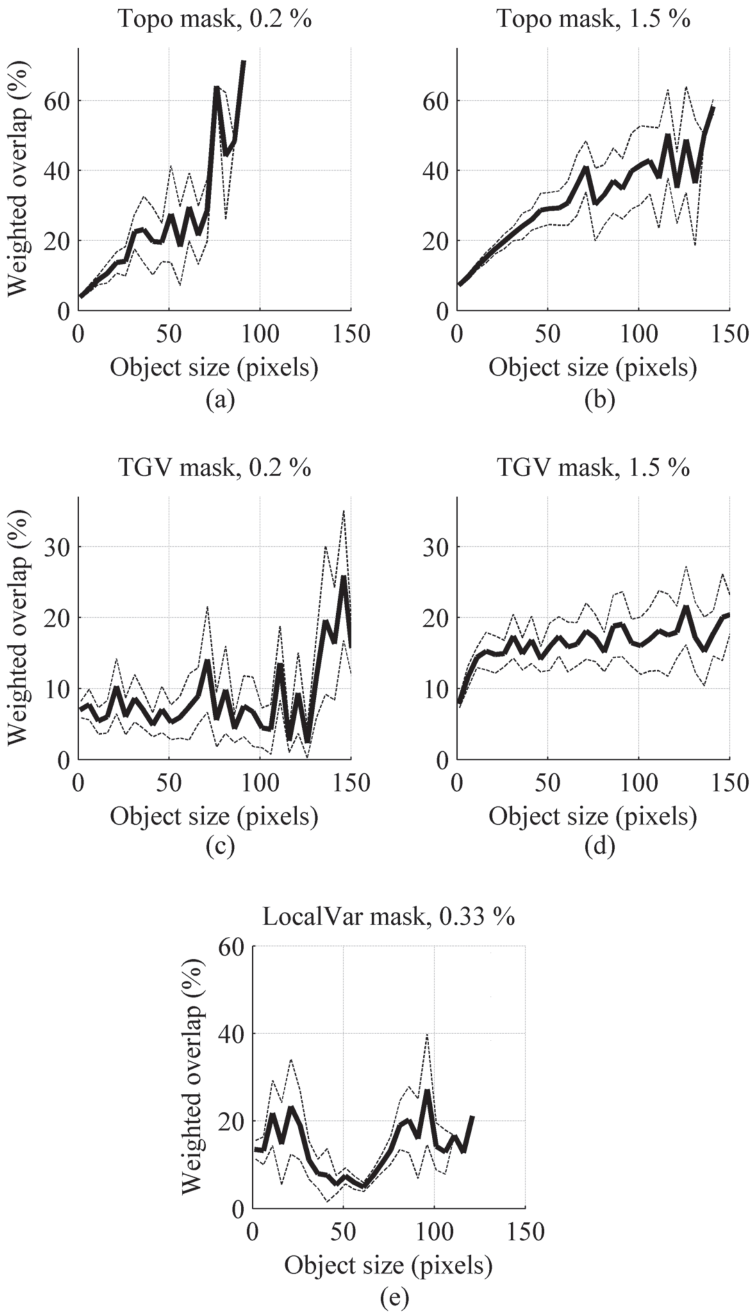

Figure 11. Overlap of the reflectance mask with the forward masks as a function of the size of objects picked from the forward masks. (a) Topo mask with $p = 0.2$ %, (b) Topo mask with $p = 1.5$ %, (c) TGV mask with $p = 0.2$ %, (d) TGV mask with $p = 1.5$ %, (e) LocalVar mask with $p = 0.33$ %. The dashed lines represent the 95 % confidence limits of the 16 non-back-trap results.

Section 4.2 showed that the mutual information between print reflectance and surface properties is not as high in the Topo mask as in the other forward masks. This may be due to the fact that Topo mask causes an abrupt edge to the space of topography observations, since the mask selects points in which the topography values fall below a certain threshold. Hence the GMMs are not able to describe the joint pdf of the surface properties and print reflectance in a similar precision as in the case of TGV and LocalVar mask points. It must also be noted that mutual information describes basically different interrelations than the plain overlap of two binary masks.

5 CONCLUSIONS

We have estimated the pointwise joint probability density functions of print reflectance and surface topography characteristics of newsprint paper printed in a sheet fed pilot offset press. We have studied the mutual relationships both throughout the observation range and in anomalous points, i.e. points with unusual topography or print reflectance. Applying GMMs and MI we have suggested a procedure to identify regions on the paper with exceptional values of topography, topography gradient and topography variance. These regions have a highly increased – at least tenfold – probability to have extremely high print reflectance, compared to randomly selected regions.

Our results have shown that topography, its gradient and its local variance all contribute to identifying the regions where the surface characteristics and print reflectance have stronger than average interdependence. Independent of the search strategy for the identification of regions with exceptional topography, the modeling results inside these regions always suggest that surface topography in combination with its local variance are the most important variables to describe the interrelation between small-scale paper surface topography and local print reflectance. We have confirmed the statistical significance of our results by showing that unrelated data with the same statistical and spatial correlation properties as the true data shows negligible values for MI compared to the interrelations revealed by our analysis.

The probabilistic approach, which does not assume an underlying mathematical model describing the interrelations between target variable, i.e. print reflectance, and its explanatory variables (e.g. topography), provides a viable alternative to the various deterministic modeling approaches that need a priori formulation of a model. The simulation methods that have been developed to prove the statistical significance of the mutual information found between the analyzed variables provide a quantitative interpretation for MI. This might contribute to a better applicability of information theoretic analysis methods in pulp and paper research.

REFERENCES

1. J.M. Fetsko and A.C. Zettlemoyer. Factors affecting print gloss and uniformity. *Tappi* **45**(8):667–681, 1962.
2. J.R. Parker. Fundamental paper properties in relation to printability. In **The Fundamental Properties of Paper Related to Its Uses**, *Trans. 5th Fund. Res. Symp.*, (ed. F. Bolam), pp517–543, BPBIF, London, 1976.
3. S.T.P. Karttunen. Structure and behaviour of a paper's surface in printing. In **The Fundamental Properties of Paper Related to Its Uses**, *Trans. 5th Fund. Res. Symp.*, (ed. F. Bolam), pp544–560, BPBIF, London, 197.
4. B. Lyne. Machine-calendering: implications for surface structure and printing properties. *Tappi J.* **59**(8):101–106, 1976.
5. I.F. Hendry. Some techniques for the assessment of coated art papers. *Tappi* **44**(10):725–731, 1961.
6. W.C. Walker and J.M. Fetsko. A concept of ink transfer in printing. *American Ink Maker* **33**(12):38–71, 1955.
7. I. Ichikawa, K. Sato and Y. Ito. A new concept of ink transfer equation. *Research Bulletin of the Government Printing Bureau*, Japan, No. 1, 1962.
8. P.J. Mangin, M.B. Lyne, D.H. Page and J.H. De Grâce. Ink transfer equations – parameter estimation and interpretation. In proc. *Adv. in Printing Science and Techn.*, (ed. W.H. Banks), Vol. 16, pp180–205, Pentech Press, London, 1982.
9. G.G. Barros. Influence of substrate topography on ink distribution in flexography. PhD Thesis, Karlstad University, Sweden, 2006.
10. I.M. Kajanto. Pointwise dependence between local grammage and local print density. *Paper and Timber* **73**(4):338–345, 1991.
11. M.A. MacGregor, P.-Å. Johansson and M.-C. Béland. Measurement of small-scale gloss variation in printed paper. In proc. *1994 Int. Printing and Graphic Arts Conf.*, pp33–43, Halifax, 1994.
12. A. Dickson. Evaluating the relationship between grammage, topography and print properties in newsprint. In proc. *60th Appita Annual Conference*, pp19–23, Melbourne, 2006.
13. H.F. Rance (ed.). Handbook of paper science. Elsevier, Amsterdam, 1982.
14. I.T. Nabney. Netlab: Algorithms for pattern recognition. Springer-Verlag, London, 2002.
15. C.M. Bishop. Pattern recognition and machine learning. Springer, Singapore, 2006.
16. R. Steuer, J. Kurths, C.O. Daub, J. Weise and J. Selbig. The mutual information: Detecting and evaluating dependencies between variables. *Bioinformatics* **18**(Suppl.2):231–240, 2002.
17. P. Hansson and P.-Å. Johansson. Topography and reflectance analysis of paper

surfaces using a photometric stereo method, *Optical Engineering* **39**(9):2555–2561, 2000.
18. L. Brown. A survey of image registration techniques. *ACM Computing Surveys* **24**(4):325–376, 1992.
19. G. Wolberg. Digital image warping. IEEE Computer Society Press, 1990.
20. M.R. Lähdekorpi, H.A.T. Ihalainen and R.K. Ritala. Using image registration and alignment to compare alternative 2D measurements. In proc. *XVIII IMEKO Word Congress*, Rio de Janeiro, 2006.
21. M.R. Mettänen, H.A.T. Ihalainen and R.K. Ritala. Alignment and statistical analysis of 2D small-scale paper property maps. *Appita Journal* **61**(4):323–330, 2008.
22. A.P. Dempster, N.M. Laird and D.B. Rubin. Maximum likelihood from incomplete data via the EM algorithm. *J. Royal Statistical Soc. Series B* **39**(1):1–38, 1977.
23. M.A.T. Figueiredo and A.K. Jain. Unsupervised learning of finite mixture models. *IEEE Trans. Pattern Analysis and Machine Intelligence* **24**(3):381–396, 2002.
24. S. Kullback. Information theory and statistics. Dover Publications, Inc., Mineola, New York, 1997.
25. P. Viola and W.M. Wells. Alignment by maximization of mutual information. *International J. of Computer Vision* **24**(2):137–154, 1997.
26. B. Zitova and J. Flusser. Image registration methods: a survey. *Image and Vision Computing* **21**(11):977–1000, 2003.
27. I. Kajanto. The effect of formation on print quality with woodfree offset papers. *Nordic Pulp and Paper Res. J.* **4**(1):8–15, 1989.

Transcription of Discussion

PROBABILISTIC ANALYSIS OF SMALL-SCALE PRINT DEFECTS WITH ALIGNED 2D MEASUREMENTS

Marja Mettänen,[1] *Ulrich Hirn*,[2] *Mikko Lauri*[1] and *Risto Ritala*[1]

[1]Department of Automation Science and Engineering, Tampere University of Technology, P.O. Box 692, 33101 Tampere, Finland
[2]Institute of Paper, Pulp and Fibre Technology, Graz University of Technology, Kopernikusgasse 24, 8010 Graz, Austria

Ilya Vadeiko FPInnovations

Thank you for a very interesting presentation and a strong approach. First question, what was the print density of your prints? Was it commercial level or somewhat different?

Marja Mettänen

The print density was from 0.9 to 1.1, the target density being 1.0. It was intended to be at a commercial level.

Ilya Vadeiko

Okay. Did you apply the high-pass filter to the prints as well as to the topography?

Marja Mettänen

No, the print reflectance images were not filtered at all.

Discussion

Ilya Vadeiko

Just a comment. Your filter had a cut of 250 µm, is that correct?

Marja Mettänen

Yes, that is the limit the wavelength.

Ilya Vadeiko

Normally, at commercial print densities, the human eye is not that sensitive to variations at such short wavelengths.

Just another comment regarding your suggestion that some particular masks applied to the topography of paper can provide good assessment of the paper surface effect on print quality. It would be interesting to introduce several other parameters like you did for the height of the topography points or for the gradient, and look for some principal directions in the multi-dimensional space of the parameters in order to better understand the optimal mask that determines the print quality.

Marja Mettänen

Thank you for the comment.

Stefan Lindström Mid Sweden University

It was nice to see a new statistical method, but I wondered if there is some objective way to discriminate whether this is a better method than using the correlation number?

Marja Mettänen

I would say that, yes, we can just use correlation. But we will not see the whole picture because there is more than linear dependence, and the modelling of the whole probability density function will give us complete information about the dependence and not only linear dependence.

We can estimate the MI using the non-Gaussian joint probability density, for instance a GMM. For comparison, we can also estimate the MI using a Gaussian pdf estimate, which corresponds to computing the correlation coefficient and transforming it into MI. There is an analytical expression for that transformation. Then, as the MI from the Gaussian assumption is smaller than the MI from GMM, this means that also the coefficient of determination, “R-squared”, is smaller in the linear model.

William Sampson University of Manchester (from the chair)

Your surface topography that you showed on the screen looked rather symmetrical – it looked Gaussian. So are the heights you are observing typical of what you see?

Marja Mettänen

I would say it is typical at least after the high pass filtering. I was kind of wondering about the distribution of the surface topography values because I had the impression that it should be log normal and not normal.

William Sampson

I think it should be skewed, yes. Kit Dodson presented a model in 2001 for pore heights in the surface, and in the bulk of the sheet, and they were effectively exponential. However, that would only end up tipping over to a gamma distribution which is like a log-normal and Ramin Farnood has data, which he has yet to publish but he will, which shows a skew distribution and I have done some simulations that would suggest the skew as well. So I think it is worth looking at what that filter is doing to the data, because it may be that it is giving you some of your MI number.

Marja Mettänen

Well, you think the filter is causing the MI?

William Sampson

Well, the filter is doing something to the distribution and the MI is quantifying the covariance between your distributions, so if one of your distributions is changing shape it might be concerning.

Marja Mettänen

Yes, thank you for the comment, I will look at that.

A further comment from the authors

The shape of the distribution of surface heights is partly explained by the technique by which the surface topography is measured. We do not use a surface profilometer but instead a camera-based system with inclined lights, i.e. photometric stereo. Our device is therefore not capable of recording the depths of the deepest surface pores as we must place the lights at a large enough angle with respect to the surface normal to have enough contrast in the images and to be able to detect subtle height variations on the paper surface. However, it was checked afterwards that the topography values do have a negative skew both before and after high-pass filtering.